Neural fields with sigmoidal firing rates: approximate solutions

Stephen Coombes and Helmut Schmidt
Department of Mathematical Sciences, University of Nottingham,
Nottingham, NG7 2RD, UK.

February 17, 2010

Abstract

Many tissue level models of neural networks are written in the language of nonlinear integro-differential equations. Analytical solutions have only been obtained for the special case that the nonlinearity is a Heaviside function. Thus the pursuit of even approximate solutions to such models is of interest to the broad mathematical neuroscience community. Here we develop one such scheme, for stationary and travelling wave solutions, that can deal with a certain class of smoothed Heaviside functions. The distribution that smoothes the Heaviside is viewed as a fundamental object, and all expressions describing the scheme are constructed in terms of integrals over this distribution. The comparison of our scheme and results from direct numerical simulations is used to highlight the very good levels of approximation that can be achieved by iterating the process only a small number of times.

1 Introduction

Neural field models have been the subject of much mathematical attention since their modern formulation in the 1970s by Wilson and Cowan [1, 2] and Amari [3, 4]. These models typically take the form of integro-differential equations and have been used to model the coarse-grained dynamics of large ensembles of neurons. The *continuum* assumption seems highly appropriate when one acknowledges the large number of neurons and synapses that reside in even a small piece of brain cortex. Such spatially extended models treat a density of neurons at a point with inputs that arise from the weighted contribution of activity at other points in the tissue. Because these interactions are mediated by long-range axonal fibres the resulting tissue-level model is inherently non-local, with a one-dimensional prototypical model being

$$\frac{1}{\alpha}u_t = -u + \psi, \qquad \psi(x,t) = \int_{-\infty}^{\infty} \mathrm{d}y w(x-y) f(u(y,t)-h). \tag{1}$$

Here $u = u(x,t)$ with $x \in \mathbb{R}$ and $t \in \mathbb{R}^+$ represents synaptic activity. The function f is often taken to be smooth and monotonically increasing ($f' > 0$) with values between 0 and 1, representing the firing rate of the tissue with a constant threshold h. The weight kernel $w(x)$, representing anatomical connectivity, will be taken to be symmetric $w(x) = w(|x|)$ and continuous with $\int_{-\infty}^{\infty} \mathrm{d}y w(y)$ finite. Finally the time-scale $\alpha > 0$ sets the rate of synaptic processing. For a review of the dynamics of (1) and other generalised neural field models we refer the reader to [5]. Much of the progress in understanding existence and stability of spatially localised and travelling

wave solutions to (1) has been made by working with a very specific choice of nonlinear firing rate function, namely the Heaviside [4, 6]. Indeed results for smooth firing rates are few and far between [7, 8]. Here we develop a novel approximation technique for treating sigmoidal firing rate shapes that exploits some of the original formalism developed by Amari for the case of a Heaviside.

2 The Amari Heaviside formalism

Time-independent solutions of (1) satisfy $\psi = u$ where

$$u(x) = \int_{-\infty}^{\infty} \mathrm{d}y w(x-y) f(u(y) - h). \tag{2}$$

Amari made the pertinent observation that for a Heaviside function localised solutions of (2) can be explicitly constructed. In the special case $f(u) = \Theta(u)$, with $\Theta(u) = 1$ for $u \geq 0$ and zero otherwise then a solution for which $R(u) = \{u(x) > h\}$ is a bounded, connected open interval defines a 1–bump. Such bumps have been linked to mechanisms for short term memory (the temporary storage of information within the brain) in pre-frontal cortex [9]. Introducing the two threshold crossings x_i, $i = 1, 2$, defined by $u(x_i) = h$ (and remembering that $w(x) = w(|x|)$, it is natural to look for symmetric 1–bump solutions with $-x_1 = \Delta = x_2$ with $\Delta > 0$ (with the origin chosen at the bump center without loss of generality). In this case we define the bump width L as $L = 2\Delta$. The solution can then be written in closed form parametrised by Δ as

$$u(x) = \int_{-\Delta}^{\Delta} \mathrm{d}y w(y-x). \tag{3}$$

The unknown Δ is then determined in a self-consistent way by demanding that the solution cross threshold at $x_{1,2}$, namely $u(x_1) = h = u(x_2)$ giving an implicit expression for L in the form $h = \int_0^L \mathrm{d}y w(y)$. Consider for example the wizard-hat $w(x) = (1 - |x|)\mathrm{e}^{-|x|}$, describing a model with short range excitation and long range inhibition. A simple calculation gives

$$u(x) = \begin{cases} g(x+\Delta) - g(x-\Delta) & x > \Delta \\ g(\Delta - x) + g(x+\Delta) & -\Delta \leq x \leq \Delta \\ g(\Delta - x) - g(-\Delta - x) & x < -\Delta \end{cases}, \tag{4}$$

where $g(x) = x\mathrm{e}^{-x}$. The conditions $u(\pm\Delta) = h$ leads to the equation $L\mathrm{e}^{-L} = h$. Hence, 1–bumps are only possible if $h < 1/\mathrm{e}$. The full branch of solutions for $L = L(h)$ is shown in Fig. 1, together with the shape of a typical 1–bump. Using an interface dynamics approach defined by the condition $u(x_i(t), t) = h$, Amari could show that it is the wider of the two solutions that is stable. The same result can also be recovered using an Evans function approach [6].

3 Sigmoidal firing rates defined via a threshold distribution

In this section we exploit the fact that a sigmoid can be viewed as a smoothed Heaviside to develop the Amari Heaviside formalism in a more general setting. From the fundamental theorem of calculus we have that $f(u) = \int^u \mathrm{d}v f'(v)$. In this way we may write a sigmoidal function f in the form

$$f(u) = \int_{-\infty}^{\infty} \rho(\xi)\Theta(u - \xi)\mathrm{d}\xi, \tag{5}$$

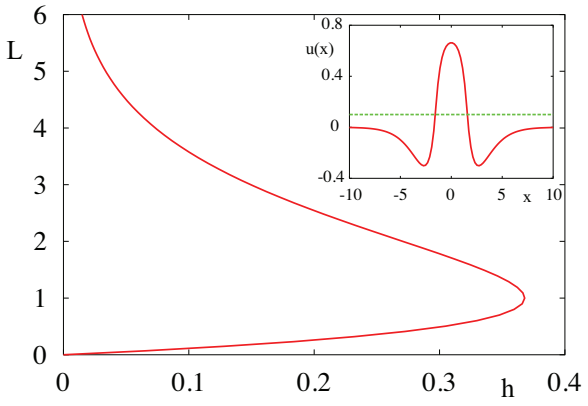

Figure 1: Bump width $L = 2\Delta$ as a function of h, as determined by $Le^{-L} = h$ for a Heaviside firing rate function and wizard hat kernel $w(x) = (1 - |x|)e^{-|x|}$. The inset shows a stable 1–bump (upper branch) at $h = 0.1$.

where $\rho = f'$. In what follows we shall fix the distribution ρ to have compact support so that $\rho(\xi) = 0$ for $\xi \ni [0, \tau]$ for some $\tau > 0$ and to be normalised such that $\int_{-\infty}^{\infty} \mathrm{d}\xi \rho(\xi) = 1$. Hence, the firing rate takes the form

$$f(u) = \begin{cases} 1 & u \geq \tau \\ \int_{-\infty}^{u} \mathrm{d}\xi \rho(\xi) & 0 < u < \tau \\ 0 & u \leq 0 \end{cases}. \tag{6}$$

The form of (6) is very natural in a neural context since many types of neurons do not fire at all below some cut-off and fire at a maximum rate (set by the refractory period) for very strong stimulus. Moreover, as we shall now show, functions of the form (6) are amenable to further mathematical analysis. Note that in the limit $\tau \to 0$ (6) approaches a Heaviside function. A smooth $C^{\infty}(\mathbb{R})$ firing rate can be generated using the choice

$$\rho(\xi) = \begin{cases} A \exp(r/(\xi(\xi - \tau))) & 0 < \xi < \tau \\ 0 & \text{otherwise} \end{cases}, \tag{7}$$

where $r > 0$ and A is set by normalisation. A piece-wise linear model is obtained for the choice

$$\rho(\xi) = \Theta(\xi)\Theta(\tau - \xi)/\tau. \tag{8}$$

Examples of firing rate functions generated from (7) and (8) are shown in Fig. 2.

4 1–bump solutions

To illustrate how to analyse models with firing rate functions (6) we first show how to generalise the analysis of section 2. The time-independent solution (2) becomes

$$u(x) = \int_0^{\tau} \mathrm{d}\xi \rho(\xi) \int_{-\infty}^{\infty} \mathrm{d}y w(x - y)\Theta(u(y) - h - \xi). \tag{9}$$

The formula (9) defines a C^1 function of x provided the connectivity function w is continuous. For a 1–bump we introduce two interface functions $x_i(\xi)$, $i = 1, 2$, defined by

$$u(x_i(\xi)) = h + \xi, \tag{10}$$

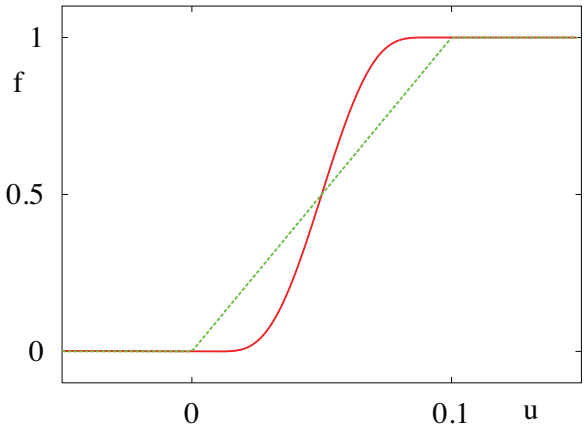

Figure 2: Firing rate functions as determined by equation (6) with $\tau = 0.1$. The solid (red) line is calculated using (7) with $r = 0.01$. Note that a Heaviside function $\Theta(u - \tau/2)$ is recovered in the limit $r \to \infty$. The dashed (green) line is calculated using (8), generating a piece-wise linear function, and is also recovered in the limit $r \to 0$ from (7).

and look for symmetric 1–bump solutions with $-x_1(\xi) = \Delta(\xi) = x_2(\xi)$ with $\Delta(\xi) > 0$ (with the origin chosen at the bump center without loss of generality). In this case we define the bump width L as $L = 2\Delta(0)$. The symmetric 1–bump solution is expressed in terms of $\Delta(\xi)$ as

$$u(x) = \int_0^\tau \mathrm{d}\xi \rho(\xi) \int_{-\Delta(\xi)}^{\Delta(\xi)} \mathrm{d}y w(y - x). \tag{11}$$

The implicit function theorem applied to the equation $u(\Delta(\xi)) = \xi + h$ shows that $\Delta : [0, \tau] \to \mathbb{R}$ is one-to-one and C^1 in an open set about $\xi = 0$ with $u(\Delta_0) = h$ and $u'(\Delta_0) \neq 0$. In this case the threshold crossing condition (10) becomes

$$h + \xi = \int_{\Delta_0}^{\Delta_c} \mathrm{d}z \frac{\rho(\Delta^{-1}(z))}{\Delta'(\Delta^{-1}(z))} \int_{-z}^{z} \mathrm{d}y w(y - \Delta(\xi)) \equiv \lambda(\Delta(\xi)), \tag{12}$$

where $\Delta_0 = \Delta(0)$ and $\Delta_c = \Delta(\tau)$. Note that by differentiation of (12) we may obtain an integral equation for Δ' in the form

$$\frac{1}{\Delta'} = \int_{\Delta_0}^{\Delta_c} \mathrm{d}z \frac{\rho(\Delta^{-1}(z))}{\Delta'(\Delta^{-1}(z))} \mathcal{D}(z, \Delta), \qquad \mathcal{D}(z, \Delta) = w(z + \Delta) - w(z - \Delta). \tag{13}$$

The hard problem is to now solve (12) or (13) for $\Delta = \Delta(\xi)$. In the limit $\tau \to 0$ where $\rho(\xi) \to \delta(\xi)$ this solution should recover the Amari Heaviside result. Hence, it is natural to develop an analysis where as a first approximation we try solutions that are valid when $\rho(\xi) = \delta(\xi)$. From (13) we see that in this case $\Delta(\xi)$ is parametrised in terms of the pair of unknown half-widths (Δ_0, Δ_c) and satisfies:

$$\Delta' = \frac{1}{\mathcal{D}(\Delta_0, \Delta)}, \qquad \Delta(0) = \Delta_0, \ \Delta(\tau) = \Delta_c. \tag{14}$$

The next order of approximation is then obtained by substitution of (14) into (12) with $\tau \neq 0$. Indeed successive approximations for $\Lambda = 1/\Delta'$ can be generated by repeating this process so that $\Lambda_n = \mathcal{H}(\Lambda_{n-1})$ where

$$\mathcal{H}(\Lambda) = \int_{\Delta_0}^{\Delta_c} \mathrm{d}z \rho(\Delta^{-1}(z)) \Lambda(\Delta^{-1}(z)) \mathcal{D}(z, \Delta), \tag{15}$$

and $(\Lambda, \Delta) = (\Lambda(\xi), \Delta(\xi))$ with $\Lambda_0(\xi) = \mathcal{D}(\Delta_0, \Delta(\xi))$. Using (12) $\Delta(\xi)$ can be reconstructed as $\Delta(\xi) = \lambda^{-1}(h + \xi)$, assuming this inverse exists. Note that λ (and hence λ^{-1}) is parametrised in terms of the pair (Δ_0, Δ_c) and all

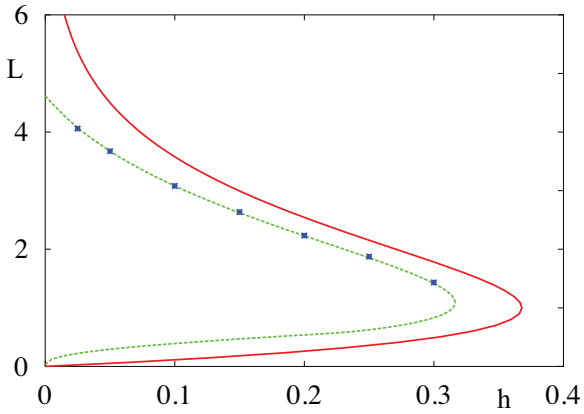

Figure 3: Bump width (first order approximation) as a function of threshold for a piecewise linear firing rate shown with dashed (green) line . (Blue) stars denote the results of numerical simulations of (1). Here $\tau = 0.1$. The outermost (red) solid curve shows the Amari (Heaviside) result, recovered for $\tau = 0$.

that remains is to determine these self-consistently. One equation for the pair (Δ_0, Δ_c) may be obtained from (12) by choosing $\xi = 0$ and another by choosing $\xi = \tau$. The simultaneous solution of this pair then completes the solution. For example at a first order of approximation we would generate the pair of equations

$$h = \int_{\Delta_c}^{\Delta_0} \Psi(z, \Delta_0) F(z, \Delta_0) \mathrm{d}z, \tag{16}$$

$$h + \tau = \int_{\Delta_c}^{\Delta_0} \Psi(z, \Delta_0) F(z, \Delta_c) \mathrm{d}z, \tag{17}$$

where

$$F(z, x) = \int_{x-z}^{x+z} \mathrm{d}y w(y), \tag{18}$$

and $\Psi(z, x) = \rho(\lambda(z) - h)[w(x - z) - w(x + z)]$.

4.1 Example

As an explicit example for which we may perform the integrals in (16) and (17) by hand consider the choice (8), defining a piece-wise linear firing rate function, and the wizard-hat function used in section 2. Introducing the function:

$$\mathcal{F}(x, y) = \frac{1}{\tau} \int^{x} [w(\Delta_0 - z) - w(\Delta_0 + z)] F(z, y) \mathrm{d}z, \tag{19}$$

means that we may write (16) and (17) in the form

$$h = \mathcal{F}(\Delta_0, \Delta_0) - \mathcal{F}(\Delta_c, \Delta_0), \qquad h + \tau = \mathcal{F}(\Delta_0, \Delta_c) - \mathcal{F}(\Delta_c, \Delta_c). \tag{20}$$

A simple calculation gives $F(z, x) = (z - x)\mathrm{e}^{-|x-z|} + (z + x)\mathrm{e}^{-(x+z)}$ for $z, x > 0$, from which we may calculate (19) as listed in Appendix A. The nonlinear algebraic equations (20) may then be solved numerically for the pair (Δ_0, Δ_c). The solution branch for L as a function of the threshold is shown in Fig. 3. Comparison with direct simulations of the original neural field model (1) show excellent agreement. The numerical scheme used for this is described in Appendix B. From (11) (at a first order of approximation) we may write

$$u(x) = \frac{1}{\tau} \int_{\Delta_0}^{\Delta_c} [w(\Delta_0 + z) - w(\Delta_0 - z)] q(z, x) \mathrm{d}z, \tag{21}$$

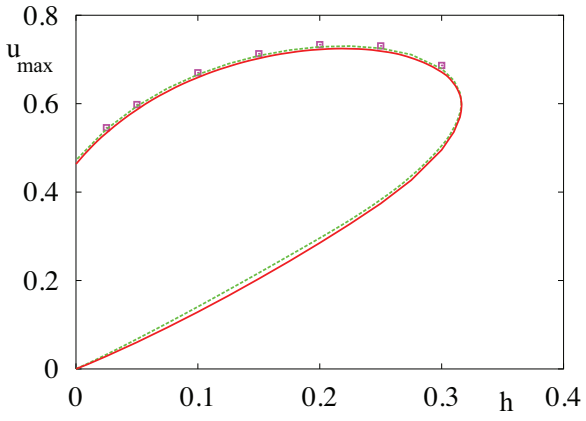

Figure 4: Bump height as a function of threshold for a piecewise linear firing rate, as for Fig. 3. Squares denote the results of numerical simulations of (1). The solid (red) line denotes the first order approximation, and the dashed (green) line shows the third order approximation.

where

$$q(z,x) = \begin{cases} g(x+z) - g(x-z) & x > z \\ g(z-x) + g(x+z) & -z \leq x \leq z \\ g(z-x) - g(-z-x) & x < -z \end{cases}, \tag{22}$$

and $g(x) = x\mathrm{e}^{-x}$. To compare how well this solution approximates the true solution we compare the amplitude $u_{\max} = u(0)$ with that obtained numerically. From (21) we have that $u_{\max} = \mathcal{G}(\Delta_c) - \mathcal{G}(\Delta_0)$, with

$$\begin{aligned} \mathcal{G}(x) &= \frac{2}{\tau}\int^{x} [w(\Delta_0 + z) - w(\Delta_0 - z)]g(z)\mathrm{d}z \\ &= \frac{\mathrm{e}^{-\Delta_0}}{\tau}\left\{(1-\Delta_0)x^2 + \frac{2x^3}{3} + \mathrm{e}^{-2x}\left[\frac{1}{4} - \frac{\Delta_0}{2} - x(\Delta_0 + x)\right]\right\}. \end{aligned} \tag{23}$$

A plot of $u_{\max}$ is shown in Fig. 4. Here we see that even at first order the approximation quantitatively captures the essential properties of the full solution, whilst going to third order there is even better agreement. The question naturally arises as to how to the performance of the algorithm changes with increasing τ. In Fig. 5 we show that the first order approximation can be relatively poor with increasing τ. However, at the third order of approximation the scheme produces excellent agreement with direct numerical simulations for all values of τ.

5 A study of periodically modulated spatial kernels

In some brain regions, and in particular the prefrontal cortex, labelling studies have uncovered a periodic modulation of anatomical connection strengths [10]. Thus it is worthwhile to focus some attention on models which incorporate such behaviour. Following a recent study by Elvin *et al.* [11] we work with the explicit choice

$$w(x) = \mathrm{e}^{-b|x|}(b\sin|x| + \cos x), \tag{24}$$

consistent with the conditions imposed in section 1. As well as the bump solutions described in sections 2 and 3 the model (1) can also support travelling wave solutions. Introducing a travelling wave coordinate $\eta = x - ct$

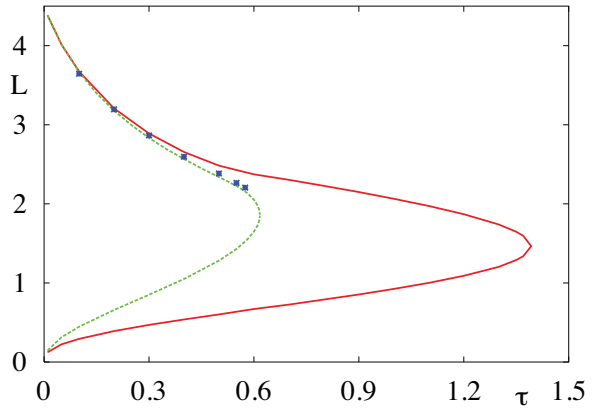

Figure 5: Bump width as a function of τ for a piecewise linear firing rate, as for Fig. 3 with $h = 0.05$. (Blue) stars denote the results of numerical simulations of (1). The solid (red) line denotes the first order approximation, and the dashed (green) line shows the third order approximation.

these are defined by bounded solutions of the integro-differential ordinary differential equation

$$-\frac{c}{\alpha}u_\eta = -u + \psi, \qquad \psi(\eta) = \int_{-\infty}^{\infty} \mathrm{d}y w(y) f(u(\eta - y) - h). \tag{25}$$

As a simple example consider a Heaviside firing rate and a travelling front with $u \geq h$ for $\eta \leq 0$ and $u < h$ for $\eta > 0$. In this case we may integrate (25) to obtain

$$u(\eta) = \mathrm{e}^{\alpha\eta/c}\left[h - \frac{\alpha}{c}\int_0^\eta \mathrm{d}\eta' \psi(\eta')\mathrm{e}^{-\alpha\eta'/c}\right], \qquad \psi(\eta) = \int_\eta^\infty \mathrm{d}y w(y). \tag{26}$$

For the solution to be bounded we require the quantity in square brackets to vanish as $\eta \to \infty$, giving an implicit expression for the wave-speed in the form

$$h = \frac{\alpha}{c}\int_0^\infty \mathrm{d}\eta' \psi(\eta')\mathrm{e}^{-\alpha\eta'/c} = \widetilde{w}(0) - \widetilde{w}(\alpha/c), \tag{27}$$

where $\widetilde{w}$ is the Laplace transform of w:

$$\widetilde{w}(\lambda) = \int_0^\infty \mathrm{d}y w(y)\mathrm{e}^{-\lambda y} = \frac{2b + \lambda}{(b+\lambda)^2 + 1}. \tag{28}$$

For a sigmoidal function defined by (6) the above argument may be extended along the lines of section 4 to give the more general result

$$\psi(\eta) = \int_0^{\Delta_c} \mathrm{d}z \frac{\rho(\Delta^{-1}(z))}{\Delta'(\Delta^{-1}(z))}\int_\eta^\infty \mathrm{d}y w(y - z), \tag{29}$$

with

$$h + \xi = \mathrm{e}^{\alpha\Delta(\xi)/c}\left[h - \frac{\alpha}{c}\int_0^{\Delta(\xi)} \mathrm{d}\eta' \psi(\eta')\mathrm{e}^{-\alpha\eta'/c}\right] \equiv \phi(\Delta(\xi)). \tag{30}$$

Here without loss of generality we have fixed $\Delta_0 = 0$ (exploiting translation invariance). Note by differentiation of (30) we also have that

$$\frac{1}{\Delta'} = \frac{\alpha}{c}[\phi(\Delta) - \psi(\Delta)]. \tag{31}$$

The solution for $\Delta(\xi)$ is parametrised in terms of the pair (c, Δ_c), which we may solve for using the analogous approximation scheme to that described in section 4. In this case successive approximations for $\Lambda = 1/\Delta'$ are

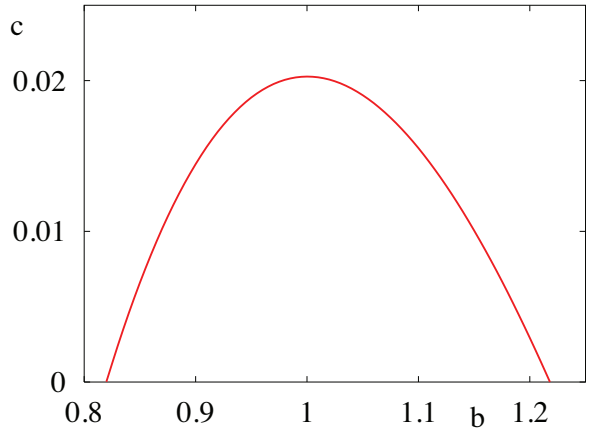

Figure 6: Wave front speed as a function of b with $h = 0.93$ for the modulated model with a piece-wise linear firing rate function and $\tau = 0.1$ (first order approximation). Note that stationary fronts occur at around $b = 0.82$ and $b = 1.22$.

generated by $\Lambda_n = \mathcal{H}(\Lambda_{n-1})$ where

$$\mathcal{H}(\Lambda) = \frac{\alpha}{c}\left[\phi(\Delta) - \int_0^{\Delta_c} \mathrm{d}z\rho(\Delta^{-1}(z))\Lambda(\Delta^{-1}(z))\mathcal{D}(z,\Delta)\right], \tag{32}$$

and

$$\mathcal{D}(z,\Delta) = \int_\Delta^\infty \mathrm{d}y w(y-z), \qquad \Lambda_0(\xi) = \frac{\alpha}{c}\left[h + \xi - \mathcal{D}(0,\Delta(\xi))\right]. \tag{33}$$

The pair of equations that define (c, Δ_c) are obtained from (26) with ψ given by (29) by demanding boundedness of solutions and setting $\xi = \tau$ in (30):

$$h = \int_0^{\Delta_c} \mathrm{d}z \frac{\rho(\Delta^{-1}(z))}{\Delta'(\Delta^{-1}(z))}\left\{\widetilde{w}(z;0) - \widetilde{w}(z;\alpha/c)\right\}, \tag{34}$$

$$h + \tau = \int_0^{\Delta_c} \mathrm{d}z \frac{\rho(\Delta^{-1}(z))}{\Delta'(\Delta^{-1}(z))}\left\{\widetilde{w}(z-\Delta_c;0) - \widetilde{w}(z-\Delta_c;\alpha/c)\right\}, \tag{35}$$

where $\widetilde{w}(z;\lambda) = \int_0^\infty \mathrm{d}y w(y-z)\mathrm{e}^{-\lambda y}$. Note that for $\tau = 0$ this pair of equations recovers the result (27) as expected.

In Fig. 6 we plot the speed of a front obtained with the scheme above at a first order of approximation. Once again we find excellent agreement with results obtained from direct numerical simulations of the full model (not shown). It is also possible to revisit the study of bumps described in section 4 for the spatial kernel defined by (24). Without listing the necessary integrations to fully describe these calculations we simply show results of a third order approximation in Fig. 7. As originally observed in [11] (for a model with a smooth firing rate and results obtained with a mixture of analysis and numerics) we also see the presence of a *gap* where (stable) 1–bump solutions do not exist. Interestingly this gap is defined by values of b which coincide with stationary front solutions (see Fig. 6). Hence homoclinic solutions to the fixed point at the origin (1–bumps) can be destroyed in favour of heteroclinic connections (stationary fronts connecting $u = 0$ and $u = 1$) in a co-dimension two bifurcation.

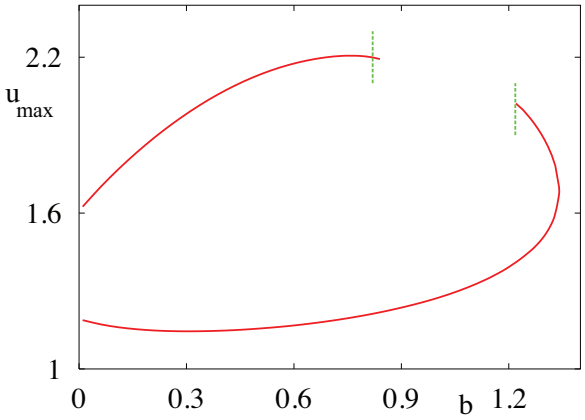

Figure 7: Solution curves (first order approximation) of 1–bump orbits as a function of b with parameters as in Fig. 6. For these parameter values there is a clear *gap*, with borders at $b \sim 0.82$ and $b \sim 1.22$, where no stable 1–bump solutions exist.

6 Discussion

In this paper we have shown how to approximate stationary and travelling wave solutions of nonlocal (integro-differential) neural field models that have a firing rate which is a smoothed version of a Heaviside. In particular we have focused on the case that this function is zero below one cut-off and equal to one above another. The connection between these two states can have arbitrary shape. Although we have not been able to deal with more general firing rate functions we have made a significant step away from the oft studied case of a pure Heaviside. The comparison with direct numerical simulations of the full model has been used to highlight the effectiveness of our scheme and that relatively few iterations (see Fig. 5) are needed to achieve good agreement. However, we have neither presented error estimates for our scheme nor proved its convergence, though we expect that the latter can be established using an appropriate (Banach or Schauder) fixed point theorem. Since the stability of stationary and travelling solutions can be determined for a Heaviside firing rate using an Evans function [6], it is natural to believe that this can be generalised to cover the firing rates considered here. However, in this case it would be a major challenge to first prove the existence of an Evans function before showing that one could construct a sequence of functions that would converge to it. These remain as interesting open problems for the mathematical neuroscience community. One important application of this work would be in the construction of so-called *snaking* diagrams for multi-bump solutions, as seen in [12] for a model with a sigmoidal firing rate function and wizard-hat connectivity. In this case we might hope to parallel the insights about pattern forming mechanisms obtained by Chapman and Kozyreff [13], who used exponential asymptotics to construct snakes-and-ladders bifurcation curves for the Swift-Hohenberg equation.

Acknowledgments

The authors would like to thank Carlo Laing for interesting conversations held during the completion of this work.

Appendix A

Calculation of (19) in section 4.1 gives

$$\mathcal{F}(x,y)=\begin{cases}\frac{1}{\tau}\frac{\mathrm{e}^{-(\Delta_0+y)}}{2}\Bigg[4x\left(\frac{x^2}{3}-y(\Delta_0-1)\right)+\mathrm{e}^{2x}\Bigg[\frac{\Delta_0-y}{2} & \\ +(x-y)(x-\Delta_0)\Bigg] & \\ -\mathrm{e}^{-2x}\left[\frac{\Delta_0-y}{2}+(x+y)(x+\Delta_0)\right]\Bigg] & x\leq y \\ \frac{1}{\tau}\frac{\mathrm{e}^{-(\Delta_0+y)}}{2}\Bigg[x^2\left(\frac{2x}{3}-(\Delta_0-1)\right)\left(1+\mathrm{e}^{2y}\right) & \\ +xy\Big(x-2\left(\Delta_0-1\right)\Big)\left(1-\mathrm{e}^{2y}\right)-\mathrm{e}^{-2x}\Bigg[\frac{\Delta_0-y}{2}\left(1+\mathrm{e}^{2y}\right)+ & \\ \Big(x\left(1+\mathrm{e}^{2y}\right)+y\left(1-\mathrm{e}^{2y}\right)\Big)\left(x+\Delta_0\right)\Bigg]\Bigg] & x>y.\end{cases} \tag{36}$$

Appendix B

For the case of the wizard-hat connectivity function given by $w(x)=(1-|x|)\mathrm{e}^{-|x|}$ the integro-differential model (1) can be transformed to a partial differential equation [5, 14] given by

$$\left(1-\partial_{xx}\right)^2\left(\alpha^{-1}u_t+u\right)=-4\left[f(u)\right]_{xx}. \tag{37}$$

This form is convenient for solution with a wide variety of numerical techniques. We adopt a simple finite difference approach to approximate the Laplacian ∂_{xx} (and apply the inverse matrix approximation of $(1-\partial_{xx})^2$ to both sides of (37)) and work on a finite domain of length 60 with 4000 mesh points. The resulting set of ordinary differential equations is then solved in Matlab using `ode45`.

References

[1] H R Wilson and J D Cowan. Excitatory and inhibitory interactions in localized populations of model neurons. *Biophysical Journal*, 12:1–24, 1972.

[2] H R Wilson and J D Cowan. A mathematical theory of the functional dynamics of cortical and thalamic nervous tissue. *Kybernetik*, 13:55–80, 1973.

[3] S Amari. Homogeneous nets of neuron-like elements. *Biological Cybernetics*, 17:211–220, 1975.

[4] S Amari. Dynamics of pattern formation in lateral-inhibition type neural fields. *Biological Cybernetics*, 27:77–87, 1977.

[5] S Coombes. Waves, bumps, and patterns in neural field theories. *Biological Cybernetics*, 93:91–108, 2005.

[6] S Coombes and M R Owen. Evans functions for integral neural field equations with Heaviside firing rate function. *SIAM Journal on Applied Dynamical Systems*, 34:574–600, 2004.

[7] K Kishimoto and S Amari. Existence and stability of local excitations in homogeneous neural fields. *Journal of Mathematical Biology*, 7:303–318, 1979.

[8] O Faugeras, F Grimbert, and J-J Slotine. Absolute stability and complete synchronization in a class of neural fields models. *SIAM Journal on Applied Mathematics*, 69:205–250, 2008.

[9] P S Goldman-Rakic. Cellular basis of working memory. *Neuron*, 14:477–485, 1995.

[10] J B Levitt, D A Lewis, T Yoshioka, and J S Lund. Topography of pyramidal neuron intrinsic connections in macaque prefrontal cortex (areas 9 and 46). *Journal of Comparative Neurology*, 338:360–376, 1993.

[11] A J Elvin, C R Laing, R I McLachlan, and M G Roberts. Exploiting the Hamiltonian structure of a neural field model. *Physica D*, to appear, 2010.

[12] S Coombes, G J Lord, and M R Owen. Waves and bumps in neuronal networks with axo-dendritic synaptic interactions. *Physica D*, 178:219–241, 2003.

[13] S J Chapman and G Kozyreff. Exponential asymptotics of localised patterns and snaking bifurcation diagrams. *Physica D*, 238:319–354, 2009.

[14] N A Venkov. *Dynamics of Neural Field Models*. PhD thesis, School of Mathematical Sciences, University of Nottingham, http://www.umnaglava.org/pdfs.html, 2009.